Time-Resolved Fluorescence of the Single Tryptophan Residue in Rat α-Fetoprotein and Rat Serum Albumin: Analysis by the Maximum-Entropy Method†

Myriam Gentin,‡ Michel Vincent,§ Jean-Claude Brochon,§ Alastair K. Livesey,⊥ Nicole Cittanova,*,‡ and Jacques Gallay§

Laboratoire pour l'Utilisation du Rayonnement Electromagnétique, Centre National de la Recherche Scientifique, Commissariat à l'Energie Atomique, Ministère de l'Education Nationale, Université Paris-Sud, Bâtiment 209D 91405 Orsay Cedex, France, Département de Biochimie, Unité d'Enseignement et de Recherche Biomédicale des Saints-Pères, 45, rue des Saints-Pères, 75270 Paris Cedex, France, and MRC Laboratory of Molecular Biology, Hills Road, Cambridge, U.K., and Department of Applied Mathematics and Theoretical Physics, Cambridge, U.K.

Received March 20, 1990; Revised Manuscript Received July 30, 1990

ABSTRACT: The time-resolved fluorescence emissions of the lone tryptophan residues in rat α-fetoprotein (RFP) and rat serum albumin (RSA) were studied. The total fluorescence intensity decays in both proteins were multiexponential. Analysis of the data by nonlinear least squares as a sum of discrete exponentials showed that four exponentials were needed for a satisfactory fit for both proteins. Analysis by the maximum entropy method using 150 logarithmically equally spaced exponentials yielded four well-resolved excited-state lifetime classes with barycenters and relative amplitudes values (c_i) that corresponded to those obtained from the nonlinear least-squares method. Changing the temperature affected the relative amplitudes of the lifetime classes but had little effect on the lifetime values themselves. This suggests that the four classes reflect local conformational substates that exchange slowly with respect to the time window of observation defined by the longest lifetime. The internal rotational dynamics of the tryptophan in each protein was monitored by fluorescence anisotropy decay measurements. The mobility of the tryptophan appeared to be larger and faster in RFP than in RSA. The nonlinear least-squares analysis suggests the existence of three rotational correlation times of 0.1, 3, and 55 ns for this protein. As a function of temperature, the long correlation time did not follow the Perrin's law expected for a rigid rotating body. This suggests that this correlation time may reflect not only the Brownian rotation of the whole protein but also the flexibilities of domains in the protein. For RSA a two-component model with correlation times of 0.4 and 31 ns was sufficient to describe the data. The variation of the long correlation time with temperature followed Perrin's law. The average angular displacement of the internal motion of the Trp residue was restricted in both proteins. In RFP, it increased from 15° to 20° over the temperature range 1–38 °C, in RSA it increased abruptly from 12° to 17° above 20 °C. A two-dimensional analysis of lifetimes and correlation times recently developed [Brochon, J. C., & Livesey, A. K. (1988) in *Light in Biology and Medicine* (Douglas, R. H., Moan, J., & Dall'Acqua, F., Eds.) pp 21–29, Plenum Publishing Corp., New York] was performed. The analysis confirmed the complexity of motion of the Trp residue in RFP, but it was not possible to attribute specific mobilities to the different excited-state populations. In RSA, the transition around 20 °C corresponds to the occurrence of a fast flexibility affecting the short-lifetime population.

Rat α-fetoprotein (RFP)[1] and serum albumin (RSA) are the main transport proteins in foetal serum. They both have a number of definite specific regions that can bind exogenous ligands, such as drugs, and endogenous biomolecules, such as fatty acids, estrogens, and bilirubin (Hervé et al., 1984, 1986). It has therefore been proposed that RFP could be the fetal counterpart of RSA, assuming the same transport role in the fetus as albumin has in the adult. The two proteins, which are supposed to have the same ancestral origin (Law et al. 1981), present very strong structural homologies. Both possess three similar domains that are organized by numerous disulfide bridges (Jagodinski et al., 1981). However, there exists a notable absence of disulfide bridges in RFP in the 295–396 peptide region, delineating a potentially flexible and open region between domains II and III, possibly serving as a "hinge segment" that could enhance flexible movements of domains (Morinaga et al., 1983). Both proteins also have the peculiarity of possessing only one tryptophan residue in their primary sequence (Hervé et al., 1987). A study of the dynamics of this lone Trp residue should permit comparison of the internal fluctuations in these two functionally related proteins. This has been investigated by time-resolved fluorescence measurements using the time-correlated single photon counting technique with the electron storage ring ACO (Anneau de Collision d'Orsay) as excitation source.

Materials and Methods

Protein Preparation. RFP was purified as previously described (Cittanova et al., 1974) and RSA was purchased from

† This work was partially supported by Grant CRE 879015 from the Institut National de la Santé et de la Recherche Médicale (J.G. and M.V.).

* To whom correspondence should be addressed.
‡ Unité d'Enseignement et de Recherche Biomédicale des Saints-Pères.
§ Université Paris-Sud.
⊥ MRC Laboratory of Molecular Biology and Department of Applied Mathematics and Theoretical Physics. Present address: Shell Research Limited, Thornton Research Center, P.O. Box 1, Chester CH1 3SH, U.K.

[1] Abbreviations: RFP, rat α-fetoprotein; RSA, rat serum albumin; Trp, tryptophan; MEM, maximum-entropy method; FWHM, full width at half-maximum.

0006-2960/90/0429-10405$02.50/0

Sigma Chemical Co. (St. Louis, MO) (fraction V) and used after chromatography on Bio-Gel P-100.

Fluorescence Measurements. Measurements of the intrinsic fluorescence anisotropy in vitrified medium were performed at −43 °C in 80% glycerol on a SLM 4800 spectrofluorimeter in the T-format configuration. The excitation light was selected with a monochromator (bandwidth, 4 nm) and the fluorescence emission was collected through Corning S-73 cutoff filters.

Time-resolved total fluorescence, $T(t)$, and anisotropy decays, $A(t)$, were measured on the instrument setup already described (Jameson & Alpert, 1979). The excitation pulse was provided by the electron storage ring of Orsay working at a frequency of 13.6 MHz in a single bunch mode with a usual measured FWHM of 1.4 ns. Fluorescence emission was collected through filters that are described in the specific experimental conditions. Data accumulation was typically stopped when 10^5 counts were stored in the peak channel of the total intensity decay curve. In some experiments 3×10^5 counts were cumulated. The apparatus response function, $E(t)$, was measured with a scattering glycogen solution at the emission wavelength.

Data Analysis. Analysis of $T(t)$ and of $A(t)$ as a sum of exponentials was performed either by a nonlinear least-square procedure (Grinvald & Steinberg, 1974; Wahl, 1979) or by MEM for which the excited-state lifetime and/or correlation time components are equally spaced on a logarithmic scale (Brochon & Livesey, 1988; Livesey et al., 1987; Livesey & Brochon, 1987).

The principles of MEM as applied to time-resolved fluorescence are outlined in the following. With vertically polarized excitation light, the parallel $I_{vv}(t)$ and perpendicular $I_{vh}(t)$ components of the fluorescence intensity at time t are

$$I_{vv}(t) = (1/3)E_\lambda(t)^* \int_0^\infty \int_0^\infty \int_{-0.2}^{0.4} \gamma(\tau,\theta,A) e^{-t/\tau}(1 + 2Ae^{-t/\theta})\, d\tau\, d\theta\, dA \quad (1)$$

and

$$I_{vh}(t) = (1/3)E_\lambda(t)^* \int_0^\infty \int_0^\infty \int_{-0.2}^{0.4} \gamma(\tau,\theta,A) e^{-t/\tau}(1 - Ae^{-t/\theta})\, d\tau\, d\theta\, dA \quad (2)$$

where $E_\lambda(t)$ is the temporal shape of the excitation flash, * denotes a convolution product, and $\gamma(\tau,\theta,A)$ is the number of fluorophores with fluorescence lifetime τ, rotational correlation time θ, and initial anisotropy A. Since the experimental data are noisy and finite in extent, there is strictly an infinite set of $\gamma(\tau,\theta,A)$ solutions within the experimental error. We then choose the distribution that maximizes the Skilling–Jaynes entropy function (Jaynes, 1983; Livesey & Skilling, 1985):

$$S = \int_0^\infty \int_0^\infty \int_{-0.2}^{0.4} \gamma(\tau,\theta,A) - m(\tau,\theta,A) - \gamma(\tau,\theta,A) \log \gamma(\tau,\theta,A)/m(\tau,\theta,A)\, d\tau\, d\theta\, dA \quad (3)$$

where $m(\tau,\theta,A)$ is a starting model for the distribution that is flat in log (τ,θ) and A space if the experimenter has no a priori knowledge about the τ values expected (Livesey & Brochon, 1987). It has been shown that this choice has at least two compelling features: (i) it introduces the minimum correlation between τ, θ, and A; (ii) the recovered $\gamma(\tau,\theta,A)$ is smooth, positive, unique, and robust to noise (Brochon & Livesey, 1987).

In this study, a fixed value of A was chosen equal to the fundamental anisotropy value measured in vitrified medium and the analyses were performed starting with 40 lifetimes (ranging from 0.05 to 20 ns) and 40 correlation times (ranging from 0.05 to 100 ns). A global analysis of $I_{vv}(t)$ and $I_{vh}(t)$ was performed.

In principle, such an analysis allows detection of the possible cross-correlations between the excited-state lifetime of the fluorophore in a given protein conformational substate and its rotational correlation time in that particular transient substate. However, there is an inherent limit to the experimental method, since the parallel and the perpendicular components of the polarized decay (expression 1 and 2) are functions of two-exponential series, the first with time constant τ_i, the excited-state lifetime of the fluorophore i, and the second with time constant κ_i, depending on both τ_i and θ_i (the rotational correlation time):

$$1/\kappa_i = 1/\tau_i + 1/\theta_i \quad (4)$$

Thus τ and θ can be exchanged without any modification in the resulting expressions for the parallel and perpendicular components of the polarized decay. This leads to construction of iso-κ curves on which exchanging τ and θ gives the same κ value. This limitation has been clearly pointed out in simulation studies (A. K. Livesey and J. C. Brochon, manuscript in preparation).

If we are only interested in the determination of the total intensity decay parameters, we can considerably simplify the analysis by summing the parallel and perpendicular components:

$$T(t) = I_{vv}(t) + 2\beta I_{vh}(t) = E_\lambda(t)^* \int_0^\infty \alpha(\tau) e^{-t/\tau}\, dt \quad (5)$$

where β is a correction factor (Wahl, 1979) and $\alpha(\tau)$ is the lifetime distribution given by

$$\alpha(\tau) = \int_0^\infty \int_{-0.2}^{0.4} \gamma(\tau,\theta,A)\, d\theta\, dA \quad (6)$$

In order to ensure our recovered distribution agrees with the data, we maximize S:

$$S = \int_0^\infty \alpha(\tau) - m(\tau) - \alpha(\tau) \log \frac{\alpha(\tau)}{m(\tau)}\, d\tau \quad (7)$$

subject to the following constraint

$$\sum_{k=1}^{M} \frac{(T_k^{calc} - T_k^{obs})^2}{\sigma_k^2} \leq M \quad (8)$$

where T_k^{calc} and T_k^{obs} are the kth calculated and observed intensities. σ^2_k, the variance of the kth point, is equal to $\sigma^2_{k,vv} + 4\,\beta^2\sigma^2_{k,vh}$ (Wahl, 1979). M is the total number of observations.

The center τ_j of a single class j of lifetimes over the $\alpha(\tau_i)$ distribution is defined as

$$\tau_j = \sum_i \alpha(\tau_i)\tau_i / \sum_i \alpha(\tau_i) \quad (9)$$

the summation being performed on the significant values of $\alpha(\tau_i)$ for the j class. C_j is the normalized contribution of the lifetime class j. A lifetime domain spanning 150 equally spaced values on a logarithmic scale between 0.1 and 20 ns was routinely used in the analyses.

Results

Total Intensity Decay Measurements. The time-resolved total intensity decay of the single tryptophan residue of the rat α-fetoprotein (RFP) measured over the whole emission spectrum displays a multiexponential behavior. MEM analysis of the data shows the existence of four classes of excited-state lifetimes ranging from 0.3 to 12 ns (Figure 1). The major classes correspond to the shortest components. The four lifetime classes were observed when either 10^5 or 3×10^5

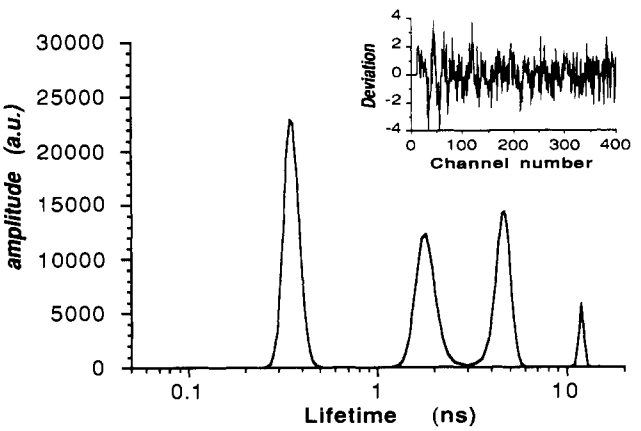

FIGURE 1: Amplitude profile of RFP total fluorescence intensity decay recovered by MEM. 10^5 counts were accumulated in the peak channel of the total intensity decay curve (corresponding to 10^7 total counts). The integrated relative amplitudes (c_i) and the barycenter of each peak (τ_i) are $c_1 = 0.42$, $\tau_1 = 0.35$ ns, $c_2 = 0.29$, $\tau_2 = 1.84$ ns, $c_3 = 0.25$, $\tau_3 = 4.59$ ns, and $c_4 = 0.03$, $\tau_4 = 12.02$ ns. $\chi^2 = 1.37$. Excitation wavelength, 300 nm; emission selected through a $CuSO_4$ cutoff filter (1 M, 1-cm optical path) and a M.T.O. A 359C wide-band filter centered at 359 nm. Temperature, 20.1 °C.

Table I: Total Fluorescence Intensity Decay Parameters of RFP and RSA[a]

c_1	c_2	c_3	c_4	τ_1 (ns)	τ_2 (ns)	τ_3 (ns)	τ_4 (ns)	$\langle\tau\rangle$ (ns)
				RFP				
0.44[b]	0.28	0.25	0.03	0.29	1.70	4.48	12.03	5.01
0.44[c]	0.27	0.26	0.03	0.30	1.68	4.34	11.72	
				RSA				
0.33[b]	0.16	0.39	0.11	0.26	2.15	5.77	9.78	6.49
0.34[c]	0.17	0.41	0.09	0.31	2.38	6.05	10.08	

[a] Excitation wavelength, 300 nm (1-nm bandwidth); emission light was selected through a 1 M $CuSO_4$ cutoff filter (1-cm optical path) and a M.T.O. wide-band filter type A 359C. Temperature, 20 °C. The optical density at 300 nm was 0.1. [b] Analysis of the data were performed by nonlinear least-squares regression using a quadruple-exponential model. [c] Analysis of the data was performed by maximum entropy with 150 lifetimes. The τ_i are the barycenters of each lifetime class calculated as described under Materials and Methods.

counts were cumulated in the peak channel of the total intensity decay curve. It can be noted that the barycenter value (τ_j) and the relative proportion (c_j) of each lifetime class agree quite closely with the respective lifetime (τ_i) and relative amplitude values (α_i) obtained from a nonlinear least-square regression analysis with a quadruple-exponential model (Table I).

Temperature variation leads to only small changes in the distribution of the lifetime classes (Figure 2). A monotonous increase of c_2 from 0.26 ± 0.02 to 0.34 ± 0.02 is observed, parallel to a decrease of c_3 from 0.26 ± 0.01 to 0.22 ± 0.01. The minor long-lifetime contribution (c_4) is not significantly changed within the range of experimental error (0.05 ± 0.02 to 0.02 ± 0.01) after temperature increase (from 1.7 to 38.8 °C). The contribution of the short-lifetime class (c_1) remains constant. Temperature increase has only a small effect on the barycenter values of each lifetime class, mainly for τ_2 (decreased by 0.6 ns) and τ_3 (decreased by 0.9 ns) (Figure 2). Moreover, no large modification of the distribution pattern for each lifetime class could be observed in the temperature range studied (data not shown). Therefore, there are only weak thermal effects on the total intensity decay parameters of RFP, suggesting that the dynamics of the fluorophore and its environment remain only marginally modified by temperature. This will be more clearly shown by the anisotropy decay data.

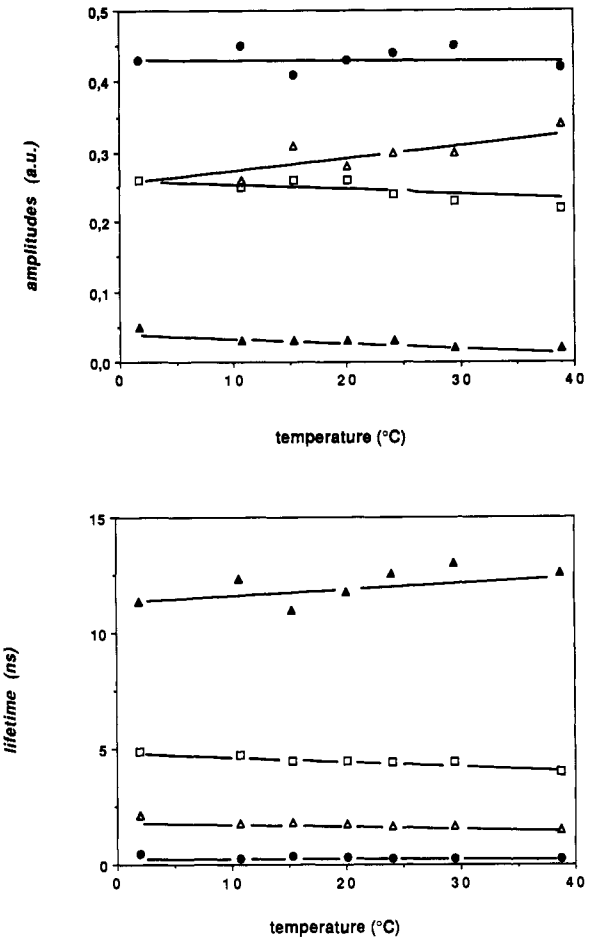

FIGURE 2: Variation of the total intensity decay parameters of RFP with temperature. Upper panel, relative integrated amplitudes; lower panel, barycenters of the excited-state lifetime classes. Experimental conditions as in Figure 1. Data were obtained by MEM analysis (Livesey & Brochon, 1987). Excitation wavelength, 300 nm; emission selected through a $CuSO_4$ cutoff filter (1 M, 1-cm optical path) and a M.T.O. A 359C wide-band filter centered at 359 nm. The same symbols were used for each particular lifetime class either for its relative contribution (upper panel) or its barycenter (lower panel).

Similar experiments were conducted on RSA. The total fluorescence intensity decay of its single tryptophan residue (Trp-214) displays, as for RFP, a multiexponential behavior. MEM analysis in the described experimental conditions of statistics and temporal resolution detects four lifetime classes ranging from 0.4 to 11 ns (Figure 3). The major contribution arises from the third class of lifetimes (barycenter of 6.15 ns at 20 °C), resulting in a long mean excited-state lifetime. The effect of temperature on the total fluorescence intensity decay parameters of RSA was also measured. No large effect can be observed on c_2. However, a change in the balance between c_1 and c_3 on the one hand and c_4 on the other occurs at temperatures higher than 20 °C (Figure 4). c_1 increases from 0.30 ± 0.01 to 0.47 ± 0.01, whereas c_3 and c_4 decrease from 0.35 ± 0.03 to 0.28 ± 0.01 and from 0.23 ± 0.05 to 0.10 ± 0.01, respectively, in the temperature range 15–33.5 °C. The temperature rise only leads to a weak effect on the barycenters of the lifetime classes but the effect is nevertheless stronger than for RFP. A small decrease of τ_3 and τ_4 values by 1.13 and 1.31 ns, respectively, can be observed (Figure 4). As for RFP, there is no large modification in the distribution pattern of the lifetime classes as a function of temperature; only sharp peaks are displayed.

Time-Resolved Fluorescence Anisotropy Decay. The fluorescence anisotropy decay of the single Trp residue of RFP

Table II: Time-Resolved Fluorescence Anisotropy Decay Parameters of the Single Tryptophan Residue of RFP as a Function of Temperature[a]

temp (°C)	β_1	β_2	β_3	θ_1 (ns)	θ_2 (ns)	θ_3 (ns)	$A_{t=0}$	χ^2
1.7		0.088 ± 0.002[b]	0.194 ± 0.001		1.24 ± 0.04	54.8 ± 1.9	0.282	1.31
	0.192 ± 0.325	0.063 ± 0.004	0.183 ± 0.008	0.08 ± 0.16	2.6 ± 0.40	67.0 ± 5.4	0.438	1.14
10.7		0.100 ± 0.002	0.182 ± 0.008		0.67 ± 0.04	49.8 ± 1.2	0.261	1.18
	0.117 ± 0.105	0.066 ± 0.004	0.168 ± 0.005	0.12 ± 0.14	3.29 ± 0.5	62.2 ± 6.0	0.351	1.07
15		0.083 ± 0.001	0.183 ± 0.001		1.32 ± 0.05	45.8 ± 1.1	0.266	1.43
	0.063 ± 0.012	0.079 ± 0.002	0.173 ± 0.002	0.21 ± 0.08	2.47 ± 0.26	54.5 ± 2.5	0.300	1.21
20.1		0.079 ± 0.002	0.173 ± 0.002		1.67 ± 0.11	44.2 ± 1.9	0.252	1.42
	0.062 ± 0.012	0.064 ± 0.006	0.156 ± 0.008	0.32 ± 0.14	3.83 ± 0.90	55.6 ± 8.2	0.282	1.21
25.3		0.083 ± 0.002	0.175 ± 0.001		1.03 ± 0.06	36.2 ± 1.1	0.258	1.53
	0.056 ± 0.004	0.063 ± 0.003	0.153 ± 0.004	0.43 ± 0.11	3.57 ± 0.51	61.4 ± 4.9	0.272	1.16
29.5		0.079 ± 0.002	0.169 ± 0.002		1.40 ± 0.09	37.2 ± 1.4	0.248	1.14
	0.063 ± 0.02	0.062 ± 0.005	0.157 ± 0.005	0.24 ± 0.16	2.77 ± 0.54	44.5 ± 3.6	0.282	1.06
38.8		0.087 ± 0.002	0.160 ± 0.002		1.11 ± 0.09	35.5 ± 1.5	0.247	1.32
	0.109 ± 0.053	0.069 ± 0.004	0.145 ± 0.004	0.1 ± 0.07	2.45 ± 0.34	45.9 ± 3.9	0.323	1.13

[a] Excitation wavelength, 300 nm. Emission, 1 M $CuSO_4$ cutoff filter (1-cm optical path) and a M.T.O. wide-band filter type A 359C. The optical density at 300 nm was 0.1. Results for two and three exponentials are given. [b] ± denotes standard deviation.

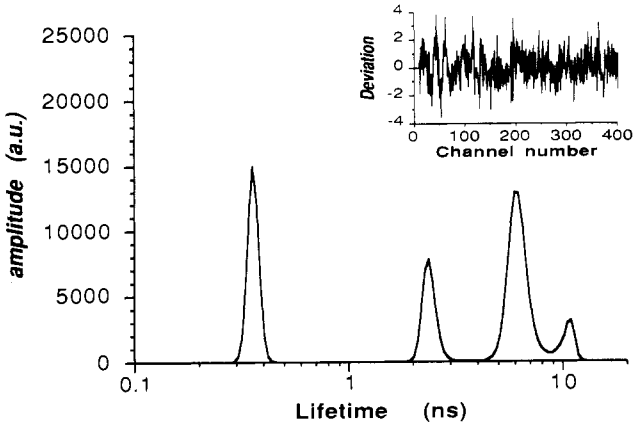

FIGURE 3: Amplitude profile of RSA total fluorescence intensity decay recovered by MEM. 10^5 counts were accumulated in the peak channel of the total intensity decay curve (corresponding to 10^7 total counts). The integrated relative amplitudes (c_i) and the barycenter of each peak (τ_i) are $c_1 = 0.30$, $\tau_1 = 0.36$ ns, $c_2 = 0.19$, $\tau_2 = 2.40$ ns, $c_3 = 0.45$, $\tau_3 = 6.24$ ns, and $c_4 = 0.07$, $\tau_4 = 10.65$ ns. $\chi^2 = 1.34$. Excitation wavelength, 300 nm, emission selected through a $CuSO_4$ cutoff filter (1 M, 1-cm optical path) and a M.T.O. A 359C wide-band filter centered at 359 nm. Temperature, 20 °C.

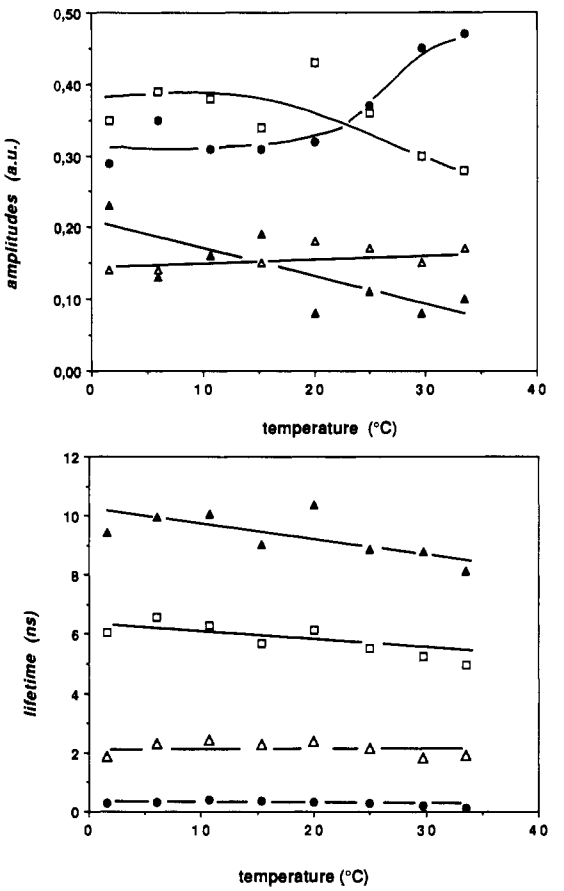

FIGURE 4: Variation of the total fluorescence intensity decay parameters of RSA as a function of temperature. Upper panel, relative integrated amplitudes; lower panel, barycenters of the excited-state lifetime classes. The same symbols were used for each particular lifetime class either for its relative contribution (upper panel) or its barycenter (lower panel).

indicates that it is the result of a rapid rotational motion superimposed on a slow one. Calculations of the anisotropy decay parameters by nonlinear least-square regression were performed with double- and triple-exponential models (Table II). The former provides an A value (anisotropy at time zero) significantly lower than the intrinsic anisotropy value measured in vitrified glycerol except for the experiments at low temperatures. The latter model leads to a better fit of the data by the χ^2 criterium and the A value is in many instances close to the one measured in vitrified medium. In this model, the short correlation time values are associated with large standard deviations and the long correlation time values are higher than in the double-exponential model.

The intermediate correlation time (θ_2) and its relative contribution to the anisotropy decay are approximately constant, using the triple-exponential calculation model, with changing temperature (Table II). On the other hand the long correlation time (θ_3) value decreases with rising temperatures and its relative contribution decreases. A plot of θ_3 versus η/T does not show a straight line crossing the η/T axis at zero value (Figure 5). Owing to the large standard deviation for the short correlation time, one cannot define a precise variation as a function of temperature.

For RSA, the double-exponential model gives an acceptable fit to the data since it provides A values close to that in vitrified medium, except for the experiments at temperatures above 25 °C (Table III). It can be seen that the contribution of the longest correlation time to the anisotropy decay is much higher for this protein than for RFP. Its variation with temperature follows the Perrin–Einstein law (Figure 5). The short correlation time value remains almost invariant with the increase in temperature.

Following the Karplus approach to describing the hindered internal rotation of the Trp residue in proteins (Ichiye & Karplus, 1983), an average angle for the fast rotation can be calculated by taking the measured value of 0.304 for the initial anisotropy at an excitation wavelength of 300 nm. For RFP, a value of about 15° continuously increasing with temperature is observed (Figure 6). For RSA, this angle is smaller below

Table III: Time-Resolved Fluorescence Anisotropy Decay Parameters of the Single Tryptophan Residue of RSA as a Function of Temperature[a]

temp (°C)	β_1	β_2	θ_1 (ns)	θ_2 (ns)	$A_{t=0}$	χ^2
1.6	0.080 ± 0.009[b]	0.245 ± 0.001	0.28 ± 0.05	60.4 ± 1.1	0.325	1.09
10.0	0.045 ± 0.030	0.247 ± 0.008	0.62 ± 0.09	45.5 ± 0.7	0.292	1.23
20.0	0.054 ± 0.007	0.245 ± 0.003	0.41 ± 0.10	30.5 ± 0.5	0.311	1.04
25	0.060 ± 0.006	0.219 ± 0.001	0.38 ± 0.07	26.2 ± 0.4	0.279	1.06
33.5	0.067 ± 0.005	0.204 ± 0.002	0.31 ± 0.10	20.3 ± 0.6	0.271	1.00

[a] Excitation wavelength, 300 nm. Emission, 1 M $CuSO_4$ cutoff filter (1-cm optical path) and a M.T.O. wide-band filter type A 359C. The optical density at 300 nm was 0.1. [b] ± denotes standard deviation.

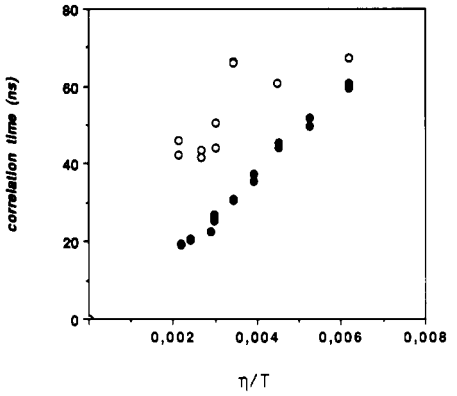

FIGURE 5: Particle rotational correlation times as a function of temperature for RFP (○) and for RSA (●). Excitation wavelength, 300 nm; emission selected through a $CuSO_4$ cutoff filter (1 M, 1-cm optical path) and a M.T.O. A 395C wide-band filter centered at 359 nm.

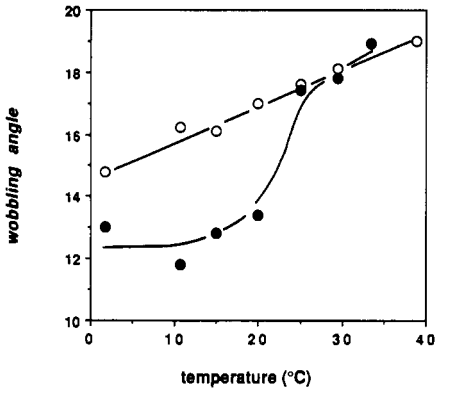

FIGURE 6: Variation of the wobbling angle of the Trp residue as a function of temperature (○) for RFP and (●) for RSA. Experimental conditions as in Figure 5.

20 °C, but above this temperature a transition occurs leading to similar value as for RFP (Figure 6).

More refined details of the dynamic properties of the Trp residues in proteins are to be expected from the two-dimensional analysis of $I_{vv}(t)$ and $I_{vh}(t)$ by MEM (Brochon & Livesey, 1988). The above nonlinear least-square regression analysis was performed by assuming identical rotational properties in each population of excited-state lifetimes. With MEM analysis, it is possible to start with a totally uncorrelated model $m(\tau,\theta,A)$, flat in log (τ,θ) and A spaces, and to delineate the distribution of correlation times through the excited-state lifetime classes. For a single chromophore, a fixed value for A is imposed in the analysis. The result is represented as a two-dimension contour plot of log τ versus log θ. However, as mentioned under Materials and Methods, extra (τ, θ) cross-peaks may be present along iso-κ curves in such a representation.

For RFP, the MEM analysis shows an apparent heterogeneity of rotational motions in the excited-state lifetime classes (Figure 7). The three major lifetime classes are clearly resolved in this analysis. The longest is not clearly detected

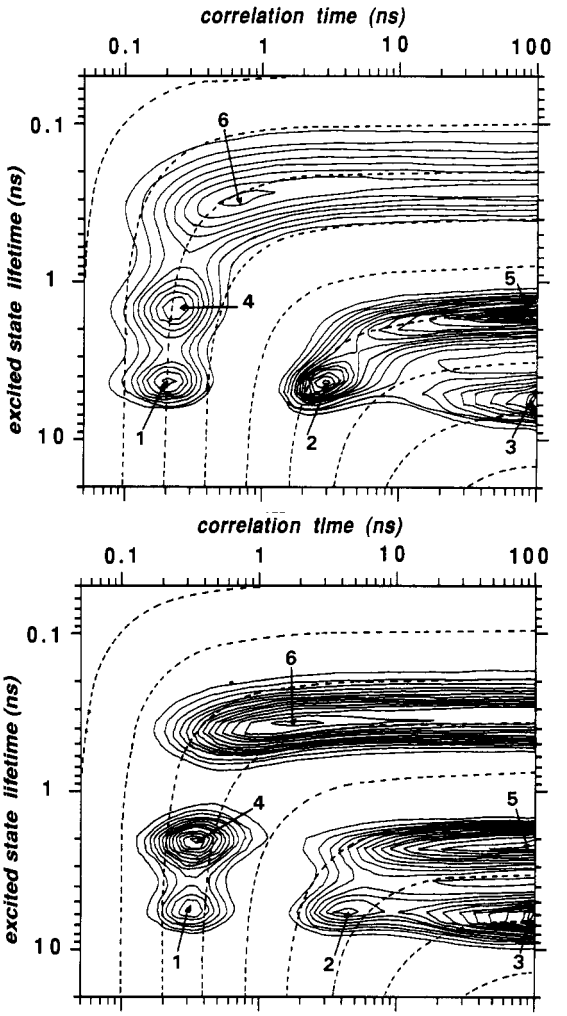

FIGURE 7: Contour plots of excited-state lifetimes versus correlation times for RFP through $\gamma(\tau,\theta,A)$ for $A = 0.300$. Upper panel, 1.7 °C; lower panel, 29.5 °C.

owing to its low contribution and to the lower time resolution of the two-dimension analysis (40 lifetimes instead of 150). A guide for reading such diagrams is that the long correlation time of the protein must affect each lifetime class in proportion to the remaining intensity of the carrier signal. Thus the overall Brownian motion of the protein will be more observable in the longest lifetime class whereas, on the contrary, the short correlation times will be observable in each lifetime class if there is no difference in motion between the excited-state populations.

From a global observation of the (τ,θ) diagram for the RFP protein, one can see that, in agreement with the nonlinear least-square regression analysis, the long correlation time of the RFP protein does not dominate the anisotropy decay, as the density of the contour lines is roughly similar in each peak of the diagram (Figure 7). Along the θ axis in the long-lifetime class (barycenter around 5 ns), two cross-peaks (labeled 1 and 2) and a trail (region 3) are evidenced. They could correspond

to three different classes of correlation times, the ill-defined trail at long correlation time values representing the overall rotation of the protein. The low definition of this cross-peak rests on the fact that the carrier signal is vanishing in this time scale (the mean excited-state lifetime is only ~4.8 ns). Peak 1 (centered at ~0.2–0.3 ns) describes the motion of the indole ring. The value of the maximum is similar to that obtained by nonlinear least-square regression. The intermediate peak (peak 2) could be the result of a slower internal motion. Examination of the iso-κ curves (dashed curves on the figure) shows that this cross-peak lies on the same curve as the broad peak (labeled peak 5) displayed in the intermediate excited-state lifetime class of barycenter around 2 ns. In fact, only two cross-peaks are displayed in this lifetime class: a broad one that arises from the overall rotation of the protein (peak 5) and the sharpest one observed in the 5-ns lifetime class displaying a maximum around 0.2–0.3 ns (peak 4). In the short lifetime class only one peak is displayed (peak 6), which can be correlated with an internal flexibility corresponding to a correlation time of around 0.75–1.5 ns (at 29.5 and 1.7 °C) superimposed on a ill-defined trail. Peak 6 makes an important contribution to the anisotropy even at low temperatures as can be seen from the density of the contour curves. However, it lies on the same iso-κ curve as cross-peaks 1 and 4 and so all these cross-peaks may reflect the same rapid flexibility in the protein. Their relative contributions decrease as a function of temperature with respect to the contribution of the long correlation time (Figure 7).

For RSA, such an analysis reveals several cross-peaks on the two-dimensional contour plots (Figure 8). From a first examination of the diagram, it is dominated by the correlation time of the protein represented by the peak displaying the densest contour areas on the two-dimensional plot (peak 1), as also deduced from the nonlinear regression analysis. The longest excited-state lifetime class is obviously the most affected by this mode of rotation (Figure 8). Almost all the anisotropy is contained in this area of the diagram at low temperatures. The value of the peak maximum is close to the correlation time value calculated from the nonlinear least-square regression. However, despite the predominance of the overall correlation time, a contribution of a fast rotation is also detectable as a cross-peak (peak 2) corresponding to a correlation time value centered around 0.4 ns at 10 °C and 0.1–0.2 ns at 33.5 °C. This rotation mode affects also the 2-ns excited-state lifetime class (peak 3). Another cross-peak (peak 4), possibly corresponding to a flexibility slower by about 1 order of magnitude, is also detectable by this analysis. It is observed mostly for the 6-ns lifetime class and its relative contribution increases as a function of temperature above 20 °C. However, this cross-peak stands on an iso-κ curve defined by the 2-ns lifetime classes and the longest correlation time. The shortest excited-state lifetime can be characterized as immobile within the protein matrix at temperature below 20 °C, since no clear maximum in the contour plot can be observed for this class of lifetimes in this temperature range. However, upon increasing the temperature, a rapid motion starts to occur, characterized by an apparent correlation time of around 0.4 ns. The corresponding cross-peak (peak 5) is on the same iso-κ curve as that resulting from the rapid flexibility (peaks 2 and 4, correlation time = 0.1–0.2 ns) already described for the 2- and 6-ns lifetime classes and can therefore be due to the same fast motion. The contributions from these cross-peaks increase sharply as a function of temperature as shown by the density of the contour curves (Figure 8).

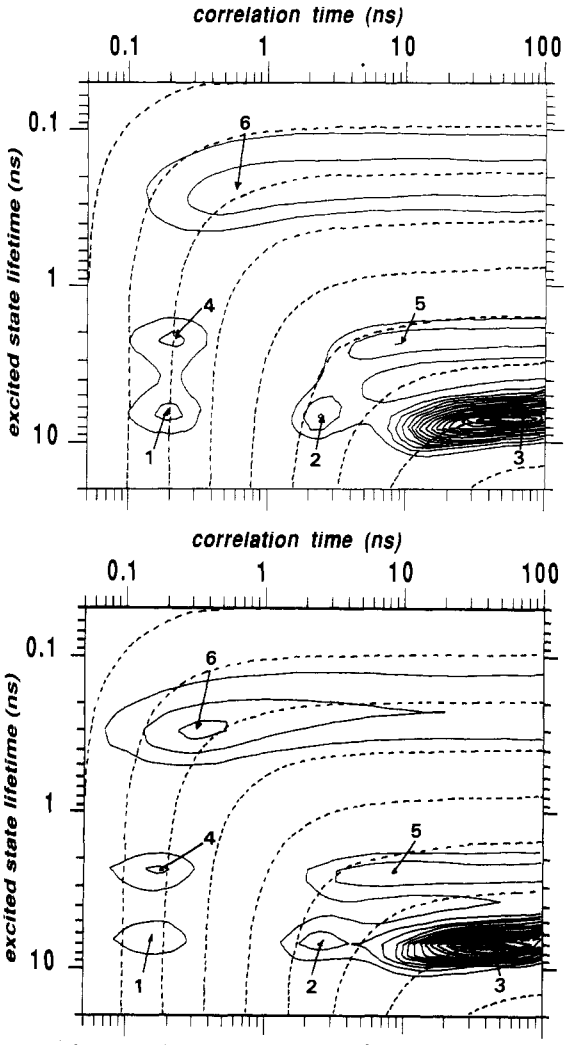

FIGURE 8: Contour plots of excited-state lifetimes versus correlation times for RSA through $\gamma(\tau,\theta,A)$ for $A = 0.300$. Upper panel, 15 °C; lower panel, 20 °C.

DISCUSSION

Experimental and theoretical studies have indicated that proteins undergo rapid fluctuations in structure and that this internal dynamics is of great importance for their biological functions: enzymatic catalysis, allosteric regulation, binding properties (Debrunner & Frauenfelder, 1982; Karplus & McCammon, 1983). From a dynamic point of view, proteins can exist under closely energetically related subconformations in equilibrium (Carreri et al., 1979). As far as protein binding functions are concerned, the internal structural fluctuations can modulate the insertion of a ligand into its specific binding site.

From the present investigation, the intrinsic fluorescence decay of the single tryptophan residue in two genetically related proteins can be interpreted as resulting from a superimposition of decays of discrete populations of Trp excited states. This provides experimental clues of local conformational heterogeneity in the close environment of the Trp residue in these two proteins. Such a picture emerges owing to the sensitivity of the tryptophan excited-state lifetime to the physical–chemical characteristics of its environment (Creed, 1984) and to the use of MEM analysis (Livesey & Brochon, 1987; Brochon & Livesey, 1987). In a preceeding paper concerning another single tryptophan containing protein—namely the horse heart apocytochrome *c* (Vincent et al., 1988)—this analytical method was proven to be a very powerful tool in detecting the existence of excited-state lifetime

heterogeneity and in discriminating between discrete and continuous broad lifetime distributions. It was in fact shown on simulated data that, provided the counting statistics were accurate enough, an image close to the simulated one can be recovered by MEM without overfitting of the data (i.e., when the analysis was stopped at the expected residual χ^2 value of the simulation). Moreover, the final images that were obtained from moderate accumulation of data after overfitting (at a χ^2 value lower by 2.5% than the expected one) and from more accumulated data without overfitting were very similar to each other. The most tricky image to recover from simulated data was the sum of n ($n > 3$) discrete exponentials for which the highest statistic level was required. In this work, experiments with large amounts of counts (3×10^5 counts in the peak channel of the total intensity decay curve) were first carried out to validate the analysis at lower statistics, in which around 10^5 counts were collected in the peak channel.

For RFP, we observed a slight but significant amplitude redistribution as a function of temperature, concerning mainly the second and the third lifetime classes. This suggests a continuous temperature-dependent shift in the equilibrium between two subconformations around the tryptophan residue. However, this thermal effect is weak, which would suggest that the dynamics of the Trp residue itself and/or of its environment are not dramatically changed in the temperature range studied. This conformational change does not influence the short excited-state lifetime class. The interactions with the proximate quencher group giving rise to this short component are likely to be as effective in all the conformations and orientations of the indole ring. The longest lifetime class barycenter is not greatly affected by temperature increase, suggesting that it corresponds to a local conformation in which the indole ring is protected from thermal fluctuations of the environment. Its contribution decreases as a function of temperature. Therefore, as was shown for the apocytochrome c protein (Vincent et al., 1988) and for the thioredoxins (Merola et al., 1989), a temperature-dependent equilibrium between different local conformational substates is likely to occur for RFP.

Similar general conclusions can be drawn in the case of RSA, although important differences in the behavior of the Trp residue are observed. There is close agreement between the values of the two lifetime components previously published for human serum albumin (Wahl & Auchet, 1972) and the two longest ones in the present study. In both proteins, the Trp residue is at position 214. In the case of human serum albumin, the longest lifetime exhibits an emission maximum around 350 nm, 10 nm to the red of the steady-state emission spectrum, which is dominated by the 6-ns component (Wahl & Auchet, 1972). This would correspond to a relaxed excited-state population.

The major temperature effect corresponds to a redistribution of the relative contribution of the shortest lifetime classes c_1 and c_3 above 20 °C. The conformational substates in which strong quenching interactions are occurring are favored by temperature increment. The long-lifetime value is more sensitive to the temperature increase than in RFP.

This result, as well as previously published results from this laboratory (Vincent et al., 1988; Merola et al., 1989), strongly suggests that instead of existing under a quasi-continuum of local conformational substates separated by low-energy barriers, these proteins display a discrete distribution of local subconformations interconverting slowly on the nanosecond time scale. This is in contrast to the interpretation assuming a priori the existence of continuous distributions of lifetimes (Alcala et al., 1987a,c), reflecting a continuous distribution of interconverting rates or a continuum of conformational substates. The interesting question is then, is the mobility of the Trp residue identical in these different conformational substates?

Anisotropy decay measurements provide direct monitoring of the rotational dynamics of the Trp residue within the protein matrix and of the Brownian motion of the protein. For both proteins, the anisotropy decay is not monoexponential; i.e., the Trp is not tightly bound to the matrix.

The classical analysis of the anisotropy decay of RFP by nonlinear least-squares regression suggests the existence of three correlation times as was also found for the flexible protein apocytochrome c (Vincent et al., 1988). The two- and three-exponential models do not provide the same value for the overall long correlation time. As a function of the viscosity/temperature ratio, its variation follows a downward curvature. Both observations suggest that this correlation time is composite: it is likely to include rotational motions corresponding to a domain and rotational motions of the whole protein.

This is in contrast to the observations on RSA. In analogous measurements, the variation of this latter protein's correlation time with η/T is a straight line as predicted by the Perrin–Einstein law. In this protein, independent motions of domains inside the protein do not seem to occur.

Comparison of the extent and rate of the local internal indole ring motions demonstrates the higher mobility of the Trp residue in RFP. A fast rotation of the indole is observable whatever the temperature, although its absolute value remains uncertain owing to the large associated standard error, whereas for RSA the fast rotation of the indole ring is three times slower. Moreover, the inclusion of an intermediate correlation time in the analysis improves the χ^2 value. It could reflect local motions of the peptide chain bearing the Trp residue. The average angle of rotation for the faster motion as calculated by using the Karplus approach (Ichiye & Karplus, 1983) is wider in RFP than in RSA below 20 °C. However, above this temperature, this angle has a similar value for both proteins. The thermal variation of the angular rotation is evidence that RSA undergoes a temperature-dependent local conformational change, also suggested from the redistribution of lifetime classes as a function of temperature.

The two-dimensional analysis, (τ,θ) confirms the high degree of internal flexibility of RFP, but it is not yet possible to ascribe a particular type of rotational motion to a given lifetime class for this protein. Nevertheless, the two-dimensional pattern may be compatible with the existence of a broad distribution of internal flexibilities affecting each excited-state lifetime population to a similar extent.

The two-dimensional analysis for RSA fully confirms that the overall correlation time of the protein dominates the anisotropy decay. It also confirms the existence of a local conformational change of the protein around the Trp residue above 20 °C. In this substate, the two-dimensional analysis shows that the Trp population exhibiting the shortest excited-state lifetimes becomes highly mobile, whereas below 20 °C it was not.

These two functionally related proteins therefore differ in their respective internal flexibilities. Such a difference in flexibility can arise from the absence of disulfide bridges in the 295–396 peptide region of RFP.

The observation that RFP is more flexible than RSA is in agreement with the picture provided by the ligand binding data. For example, a higher susceptibility of RFP than RSA to release ligands via negative cooperative binding effects has

been observed (Hervé et al., 1986). This may correspond to an adaptation process for its transport role in fetal development. The conformational differences between RFP and RSA may be at the origin of their functional differences. The greater flexibility of RFP may be responsible for the higher frequency of modulatory effects between its high-affinity binding sites, particularly with respect to that of phenylbutazone. Previous steady-state fluorescence results indicated the implication of Trp residues in the phenylbutazone binding site in both RSA and RFP but to a different extent (Hervé et al., 1987). In RSA, a direct implication resulting in a 85% quenching by the ligand was suggested, whereas only a 15% quenching was found in RFP, suggesting an indirect interaction with the Trp residue, induced by drug binding.

ACKNOWLEDGMENTS

We thank the technical staff of LURE for running the synchrotron machine during the beam-time sessions. K. Rajkowski is gratefully acknowledged for reading and criticizing the manuscript.

Registry No. L-Trp, 73-22-3.

REFERENCES

Alcala, J. R., Gratton, E., & Prendergast, F. G. (1987a) *Biophys. J. 51*, 587–596.

Alcala, J. R., Gratton, E., & Prendergast, F. G. (1987b) *Biophys. J. 51*, 597–604.

Alcala, J. R., Gratton, E., & Prendergast, F. G. (1987c) *Biophys. J. 51*, 925–936.

Brochon, J. C., & Livesey, A. K. (1988) in *Light in Biology and Medicine* (Douglas, R. H., Moan, J., & Dall'Acqua, F., Eds.) pp 21–29, Plenum Publishing Corp., New York.

Careri, G., Fasella, P., & Gratton, E. (1979) *Annu. Rev. Biophys. Bioeng. 8*, 69–97.

Cittanova, N., Grigorova, A. M., Benassayag, C., Nunez, E. A., & Jayle, M. F. (1974) *FEBS Lett. 41*, 21–24.

Creed, D. (1984) *Photochem. Photobiol. 39*, 537–562.

Debrunner, P. G., & Frauenfelder, H. (1982) *Annu. Rev. Phys. Chem. 33*, 0283–299.

Grinvald, A., & Steinberg, I. Z. (1974) *Anal. Biochem. 59*, 583–598.

Hervé, F., Rajkowski, K., Martin, M. T., Dessen, P., & Cittanova, N. (1984) *Biochem. J. 221*, 401–406.

Hervé, F., Rajkowski, K., Martin, M. T., Dessen, P., & Cittanova, N. (1986) *Biochem. J. 239*, 451–458.

Hervé, F., Martin, M. T., Rajkowski, K., Dessen, P., & Cittanova, N. (1987) *Biochem. J. 244*, 81–85.

Ichiye, T., & Karplus, M. (1983) *Biochemistry 22*, 2884–2893.

Jagodzinski, L. L., Sargent, T. D., Yang, M., Glackin, C., & Bonner, J. (1981) *Proc. Natl. Acad. Sci. U.S.A. 78*, 3521–3525.

Jameson, D. M., & Alpert, B. (1979) in *Synchrotron Radiation Applied to Biophysical and Biochemical Research* (Castellman, A., & Quercia, I. F., Eds.) pp 183–201, Plenum, New York.

Jaynes, E. T. (1983) in *Papers on Probability Statistics and Statistical Physics* (Rosenkrantz, R. D., Ed.) D. Reidel, Dordrecht.

Karplus, M., & McCammon, J. A. (1983) *Annu. Rev. Biochem. 53*, 263–300.

Law, S. W., & Dgaiczyk, A. (1981) *Nature 291*, 201–205.

Livesey, A. K., & Skilling, J. (1985) *Acta Crystallogr. A41*, 113–122.

Livesey, A. K., & Brochon, J. C. (1987) *Biophys. J. 52*, 693–706.

Livesey, A. K., Delahaye, M., Licinio, P., & Brochon, J. C. (1987) *Faraday Discuss. Chem. Soc. 83*, paper 14.

Merola, F., Rigler, R., Holmgren, A., & Brochon, J. C. (1989) *Biochemistry 28*, 3383–3398.

Morinaga, T., Sakai, M., Wegmann, T. G. & Tamaoki, T. (1983) *Proc. Natl. Acad. Sci. U.S.A. 80*, 4604–4608.

Vincent, M., Brochon, J. C, Merola, F., Jordi, W., & Gallay, J. (1988) *Biochemistry 27*, 8752–8761.

Wahl, Ph. (1979) *Biophys. Chem. 10*, 91–104.

Wahl, Ph., & Auchet, J. C. (1972) *Biochim. Biophys. Acta 285*, 99–117.